Hertz-Level Clock Spectroscopy of ^{171}Yb Atoms in a One-Dimensional Optical Lattice *

Meng-Jiao Zhang(张梦娇)[1,2], Hui Liu(刘慧)[1,2], Xi Zhang(张曦)[1,2], Kun-Liang Jiang(姜坤良)[1,2], Zhuan-Xian Xiong(熊转贤)[1**], Bao-Long LÜ(吕宝龙)[1], Ling-Xiang He(贺凌翔)[1]

[1]*Key Laboratory of Atomic Frequency Standards, Wuhan Institute of Physics and Mathematics, Chinese Academy of Sciences, Wuhan 430071*

[2]*University of Chinese Academy of Sciences, Beijing 100049*

(Received 9 March 2016)

An ultra-narrow spectroscopy of clock transition with high signal-to-noise ratio is crucial for a high-performance atomic optical clock. We present a detailed study about how to obtain a Hertz-level clock transition spectrum of ^{171}Yb atoms. About 4×10^4 atoms are loaded into a one-dimensional optical lattice with a magic wavelength of 759 nm, and a long lifetime of 3 s is realized with the lattice power of 1 W. Through normalized shelving detection and spin polarization, ^{171}Yb clock spectroscopy with a Fourier-limited linewidth of 5.9 Hz is obtained. Our work represents a key step toward an ytterbium optical clock with high frequency stability.

PACS: 06.30.Ft, 32.30.Jc, 37.10.Jk DOI: 10.1088/0256-307X/33/7/070601

In recent years, atomic optical clocks based on alkaline-earth (-like) elements such as strontium (Sr) and ytterbium (Yb) have made remarkable progress in stability and accuracy reaching 10^{-18} level,[1–3] which opens up a new chapter on a variety of fundamental research such as testing of fundamental constant variation,[4,5] hunting for topological dark matter[6] and clock-based geodesy.[7] Generally the stability of atomic clocks is characterized by the Allan deviation $\sigma_y = \frac{\Delta\nu}{\nu_0}\sqrt{\frac{T_c}{\tau \cdot N}}$, where $\Delta\nu$ is the spectroscopic linewidth of the clock system, N is the total number of atoms, T_c is the time required for a single measurement cycle, and τ is the averaging period.[8] Detailed study of how to obtain an ultra-narrow clock transition spectrum with a high signal-to-noise ratio (SNR) is crucial for a stable clock. A magic-wavelength optical lattice[9] must be employed. Through confining atoms in the Lamb–Dick region of the lattice, the first-order Doppler shift and recoil shift can be suppressed. Light shift of the clock transition induced by the lattice laser can also be cancelled at magic wavelength. Additionally, interrogating a large number of atoms simultaneously provides a high SNR far superior to single ion optical clocks.

Yb is a good candidate for the next generation of frequency standard. The ^{171}Yb atoms have a doubly forbidden transition with a natural linewidth less than 10 mHz which is insensitive to magnetic field, and the blackbody radiation shift of ^{171}Yb[10] at rt is just one half of ^{87}Sr. The ^{171}Yb atoms have the most simple hyperfine structure due to the nuclear spin of 1/2, thus the tensor light shift is zero, and highly efficient spin polarization is easier to realize compared with ^{87}Sr. In this Letter, we present a detailed experimental study on the realization of Hertz-level clock spectroscopy of ^{171}Yb atoms confined in the 1D optical lattice. Through normalized shelving detection and spin polarization, the ^{171}Yb clock spectroscopy with a Fourier-limited linewidth of 5.9 Hz is obtained.

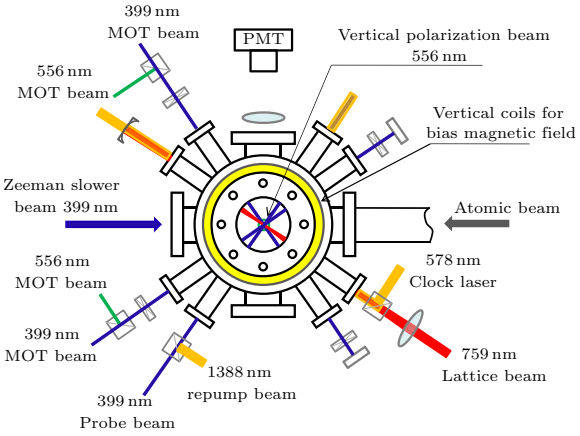

Fig. 1. Top view of the experimental setup. MOT beams along the vertical direction are not shown for clarity. The clock, lattice, repump and probe beams all are settled in the horizontal plane. The lattice beam and the clock beam are linearly polarized parallel to the bias magnetic field which is oriented at the vertical direction. The photomultiplier tube (PMT) is used to collect the 399 nm fluorescence signals.

The experimental apparatus used in our experiment is essentially the same as in our previous experiments.[11–13] The top view of our experiment setup is depicted in Fig. 1. The lattice beam, clock beam, repump beam and probe beam all are settled in the horizontal plane. The 556 nm laser used for spin polarization is oriented at the vertical direction and overlapped with the vertical MOT beam, which

*Supported by the National Natural Science Foundation of China under Grant Nos 61227805, 91536104 and 11574352.

**Corresponding author. Email: zxxiong@wipm.ac.cn

© 2016 Chinese Physical Society and IOP Publishing Ltd

is also parallel to the bias magnetic field. The rotation direction of the spin polarization beam is controlled by a liquid crystal variable retarder. The lattice laser is produced by a continuous Ti:sapphire laser working at 759.5 nm magic wavelength.[14] The lattice beam is transferred though a high power polarization maintaining fiber to the vacuum chamber, and focused to a waist radius of about 23 μm by an achromatic lens with 30 cm focal length. The maximum lattice power is about 1 W controlled by acousto-optic modulators (AOM). The lattice beam is retro-reflected by a concave mirror with a curvature radius of 200 mm to form the 1D lattice. After two cascaded MOTs, about 2×10^6 ^{171}Yb atoms with the temperature of about 20 μK are trapped in the green MOT operated on $^1S_0$–$^3P_1$ transition at 556 nm. The atom number and the temperature are measured by using standard absorption image and time-of-flight methods, respectively. To increase the transferring efficiency from the green MOT to the 1D lattice, magnetic compression is applied to match the size of the green MOT and the lattice. The gradient of the quadrupole magnetic field is increased linearly from 4 G/cm to 16 G/cm in 100 ms. The cold atoms are then transferred into the optical lattice by simply turning off 556 nm MOT beams and the quadrupole magnetic field while the lattice beam is kept on all the time. The temperature of atoms slightly increased during transferring due to the −1 MHz light shift of 556 nm transition in 759 nm lattice field at a typical power of 1 W. Finally we trapped about 4×10^4 ^{171}Yb atoms in the lattice, corresponding to 2% transfer efficiency.

The $^1S_0$–$^3P_0$ clock transition of ^{171}Yb is doubly forbidden in spin and angular momentum in principle, while due to the slight overlap among $^1P_1$, $^3P_1$ and $^3P_0$ states, this weak transition has a natural linewidth of less than 10 mHz. Thus an ultra-narrow clock laser is crucial to obtain a high-Q clock transition. Our clock laser is generated by frequency doubling a 1156 nm semiconductor laser to 578 nm, and the linewidth of the clock laser is suppressed to about 2 Hz by locking the seed laser to a high-finesse optical cavity with the Pound–Drever–Hall method. The output of the clock laser is divided into three parts and is sent to a wavelength meter, the atoms system and an optical frequency comb, respectively. As shown in Fig. 1, the 578 nm laser beam sent to the atoms system coincides with the lattice beam on the horizontal plane and covers the atoms trapped in the lattice. To decrease the mismatch between the wave vectors of the clock beam and the lattice beam, the clock beam is collimated and the waist radius is expanded to 2 mm. The clock laser frequency is controlled by an acousto-optic modulator (AOM) with a double-pass configuration. To minimize the frequency noise from fibers, the fiber noise cancellation technique[15] is applied in the fiber transportation of the clock laser, and the frequency fluctuation induced by fibers is suppressed to mHz level.

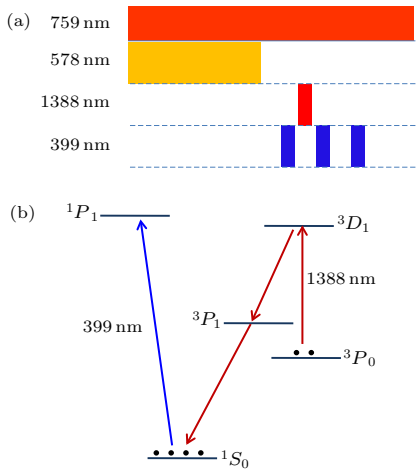

Fig. 2. (a) Time sequence of normalized shelving detection of clock excitation fraction. (b) The energy level diagram of Yb relevant to the clock interrogation. The frequency of the 1388 nm repump laser is calibrated by using a high-resolved wavelength meter with the resolution of 1 MHz. To homogeneously excite atoms, the waist of the 399 nm probe beam is designed to be about 1 mm, and the power is about 3 mW corresponding to a saturation parameter of about 3.

Directly measuring the fluorescence signal of clock transition is unrealistic due to the fact that the scattering rate is very small, thus a normalized shelving detection scheme has been adopted.[16] The detection sequence is depicted in Fig. 2(a). When the clock excitation is completed, three 5 ms pulses resonant to the strong cooling transition at 399 nm are applied and the introduced fluorescence signals are simultaneously collected with a photomultiplier tube (PMT). Each signal is then digitalized and integrated. The first measurement N_1 gives the number of atoms remaining on the ground state $^1S_0$ after clock excitation, and it also clears these atoms away. Then a 1388 nm laser resonant to the $^3P_0(F = 1/2)$–$^3D_1(F = 1/2)$ transition is applied for 5 ms to pump the atoms at $^3P_0$ excited state back to the ground state through the $^3P_1$ state as shown in Fig. 2(b). Thus the subsequent second fluorescence signal N_2 gives the number of atoms excited to the $^3P_0$ state, and the last pulse is used to generate the background signal N_0. Then the excitation fraction can be expressed by $(N_2 - N_0)/(N_1 + N_2 - 2N_0)$. This method can cancel shot-to-shot atom-number fluctuation in each cycle, and can provide a precise measurement of clock excitation fraction with high SNR.

Clock interrogation time is limited by various decoherent mechanisms of clock states including the lifetime of atoms trapped in the lattice, thus a long lifetime is important to obtain an ultra-narrow spectrum. The images of the ^{171}Yb atoms trapped in the optical lattice for different holding time from 15 ms to

7 s are recorded as shown in Fig. 3(a). After holding the lattice for 15 ms, the MOT atoms fall down under gravity and are separated from the lattice beam. Through the absorption imaging, about 4×10^4 atoms are loaded into the lattice corresponding to a transfer efficiency of 2%. The number of atoms at different lattice holding times is measured as shown in Fig. 3(b). By the exponential decay fitting, the $1/e$ lifetime is about 3 s. The loss mechanism for the atoms in the lattice is complicated. Background gas collision and lattice power noise both contribute. In our vacuum chamber, the vacuum pressure is at 10^{-10} Torr order of magnitude, thus the background gas collision is not the main reason obviously. Parametric oscillation[17] will also heat atoms and will cause atoms lost when the noise frequency of lattice power is close to twice the trap oscillation frequency. The noise spectrum of the lattice power has also been measured, while no characteristic oscillation frequency is found near twice the trap oscillation frequency. Thus more works are needed to explore in depth the trap loss mechanism.

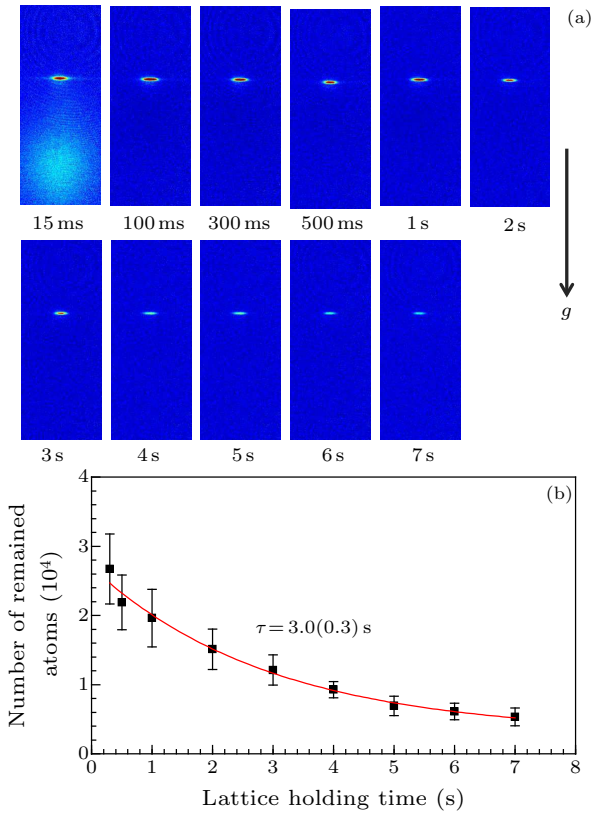

Fig. 3. (a) Images of the atoms trapped in the 1D lattice for different lattice holding times. (b) The number of atoms in lattice versus the holding time. The solid points are the measured data from the absorption images, and each data is an average of five repeated measurements. The solid line is an exponential fit, yielding a lifetime of 3.0(0.3) s.

The motional sideband spectrum with the typical carrier-sideband structure is obtained when the clock laser is scanned over the clock transition, as shown in Fig. 4. The narrow carrier peak in the center corresponding to the transition between the same longitudinal vibration states, which is free of the motional effect. The area ratio of the red sideband ($n_z \to n_z - 1$) and the blue sideband ($n_z \to n_z + 1$) indicates the temperature along the strong confined axis. Additionally, the sidebands are smeared out toward the carrier caused by the coupling between the longitudinal and transverse degrees of freedom in lattice.[18] Thus the line shape carries information about the potential depth and the longitudinal and transverse temperatures of the atoms in the lattice. The spectrum in Fig. 4 is obtained with a 100 ms Rabi pulse. The longitudinal trap frequency f_z is determined to be 103 kHz from the sharp edges of the motional sidebands, and the effective lattice depth is estimated to be $645E_{\rm rec}$, where $E_{\rm rec}$ is the lattice recoil energy. With the area ratio between the red and blue sidebands, the longitudinal temperature T_z is estimated to be about 35 μK corresponding to the average atomic population $\langle n_z\rangle \approx 3.3$. The transverse temperature $T_{\rm r} \approx 28\,\mu$K is derived by fitting the model of the sideband spectrum.[18] The longitudinal Lamb–Dick parameter $\eta_z = \sqrt{f_{\rm rec}^{\rm p}/f_z}$ is calculated to be 0.18, where $f_{\rm rec}^{\rm p}$ is the photon recoil frequency of the clock laser.

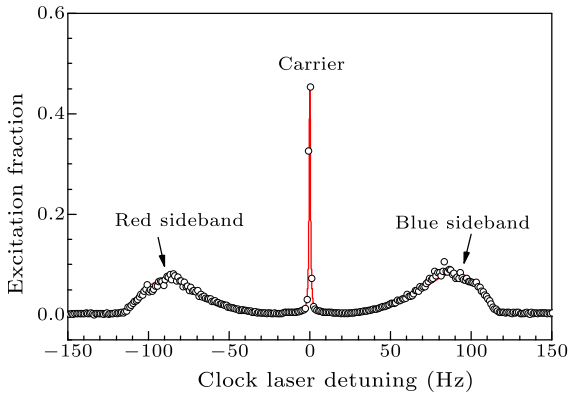

Fig. 4. The motional sideband spectrum of ^{171}Yb clock transition in the 1D lattice. The open circles are the experimental data and the red solid line is the combination of fits to the carrier and sidebands with $T_z \approx 35\,\mu$K and $T_{\rm r} \approx 28\,\mu$K. The full width at the half maximum of the carrier is 2.5 kHz.

The linewidth of the carrier in Fig. 4 is about 2.5 kHz which is much larger than the natural linewidth of the clock transition and the 9 Hz Fourier-limited linewidth corresponding to the 100 ms Rabi pulse. Obviously the power broadening effect is the main reason. When the intensity is much greater than the saturation intensity, the linewidth of clock transition is broadened by $\Gamma\sqrt{1+s}$, where Γ is the natural linewidth of clock transition, and s is the saturation parameter. To investigate the carrier linewidth dependence on the power of the clock laser, carrier linewidths at different clock laser powers are measured shown in Fig. 5. In our experiment, the $1/e^2$ waist of the clock laser is designed to about 2 mm to decrease

the inhomogeneous excitation. When the power of the clock laser is changed from 206 μW to 3 μW, corresponding to the power density from 1049 μW/cm^2 to 15 μW/cm^2, the linewidth of the carrier is decreased from 165 Hz to 75 Hz. The excitation fraction versus the power has also been measured to show a similar trend at fixed interrogation time of 100 ms. The excitation fraction increases with the power and approaches a maximum value of 0.5.

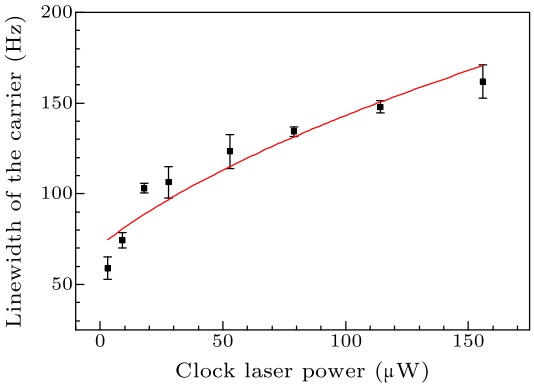

Fig. 5. The linewidth of the carrier transition versus the power of the clock laser. The error bar is from three times of independent measurements. The black filled squares are the experimental data and the red solid curve is a fitting of the power broadening formula.

With the decrease of the clock laser power, the Zeeman sublevels gradually become resolved. In Fig. 6(a), while the bias magic field is oriented at the horizontal plane and at an angle of about 55° with the propagation direction of the clock laser, all the Zeeman transition lines including two π transitions and two σ transitions can be seen. To suppress σ transitions we have carefully aligned the bias magic field along the vertical direction and parallel to the polarization of the clock laser. Then a pure π-transition spectrum can be observed as shown in Figs. 6(b) and 6(c). In this case, the atoms are uniformly distributed between two Zeeman sublevels theoretically, which limits the excitation fraction to less than 0.5. Thus the spin polarization is necessary for improving the SNR of the spectrum. Once the atoms are prepared to the same Zeeman sublevel, the SNR is doubled. Meanwhile, the collision shift and broadening will be suppressed. When a σ^- polarized 556 nm laser resonant to the $^1S_0(m_F = 1/2)$–$^3P_1(m_F = -1/2)$ transition is applied, the atoms on the $^1S_0(m_F = 1/2)$ state will be pumped to the $^1S_0(m_F = -1/2)$ state. In the same way, the atoms can also be prepared on the $^1S_0(m_F = 1/2)$ state by using the σ^+ polarized 556 nm laser resonant to the $^1S_0(m_F = -1/2)$–$^3P_1(m_F = 1/2)$ transition.

In our experiment of spin polarization, the bias magnetic field is about 1.8 G inferred from the Zeeman splitting. When the spin polarization laser is not applied, the excitation fractions of the two π transitions are comparative and less than 0.2 as shown in Fig. 6(b). When the σ^- polarized 556 nm laser is turned on for 30 ms before the clock interrogation, the left peak corresponding to the $^1S_0(m_F = 1/2)$–$^3P_0(m_F = 1/2)$ transition is suppressed to nearly zero and the right peak corresponding to the $^1S_0(m_F = -1/2)$–$^3P_0(m_F = -1/2)$ transition is increased to 0.6 shown in Fig. 6(c). The interrogation time has been optimized independently to obtain the maximum excitation fraction. Finally 95% atoms are successfully prepared into a single Zeeman sublevel.

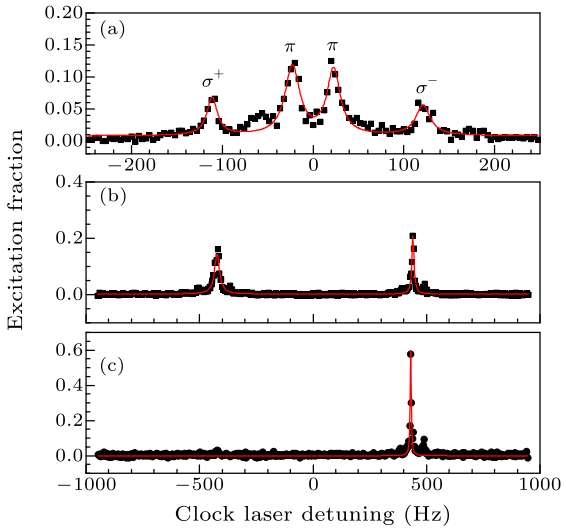

Fig. 6. Zeeman spectra of the ^{171}Yb clock transition. The black filled circles are the experimental data, and the red solid lines are the fitting curves with the Lorentz profile. (a) All the Zeeman transition lines are observed when the bias magic field is at an angle of about 55° with the vector direction of the clock laser. (b) Pure π-transition spectrum when the magnetic field is parallel to the polarization of the clock laser and the spin polarization is not applied. (c) When the 556 nm spin polarization laser is applied, only a single π-transition can be seen.

In the clock detection, the finite interrogation time leads to a limited linewidth of the clock transition corresponding to the inverse Fourier transformation of the pulse of the clock laser. In the Rabi spectrum, this Fourier-limited linewidth is derived as $\Delta\nu \approx 0.89/\tau_{\rm p}$, where $\tau_{\rm p}$ is the interrogation time.[19] By decreasing the power of the 578 nm clock laser to minimize the power broadening and meanwhile adjusting the Rabi pulse time, we finally obtained the Fourier-limited Rabi spectra of the clock transition as shown in Fig. 7.

In Fig. 7(a), a linewidth of 18(2) Hz is observed under 50 ms interrogation time which corresponds to a Fourier-limited linewidth of 17.8 Hz. When the interrogation time is increased to 80 ms, the linewidth is decreased to 11.2(1.0) Hz as shown in Fig. 7(b). In Fig. 7(c), the power of the 578 nm clock laser is finally decreased to about 1 μW, and the largest excitation fraction is observed at 170 ms. The linewidth is measured to be 5.9(0.5) Hz by the Lorentz fitting which is also close to the Fourier-limited linewidth of

about 5.2 Hz. The bare Rabi frequency is calculated to be about 9.7 Hz and the corresponding pulse time is 103 ms, which gives the largest excitation fraction theoretically. This discrepancy comes from the inhomogeneity of the Rabi excitation caused by higher atomic temperature and the mismatch of the wave vectors of lattice beam and clock beam.[18] To further narrow the clock transition in the future, more elaborate works are necessary such as further lowering the temperature of the atoms, carefully alignment of the lattice beam and clock beam, and a more stable clock laser.

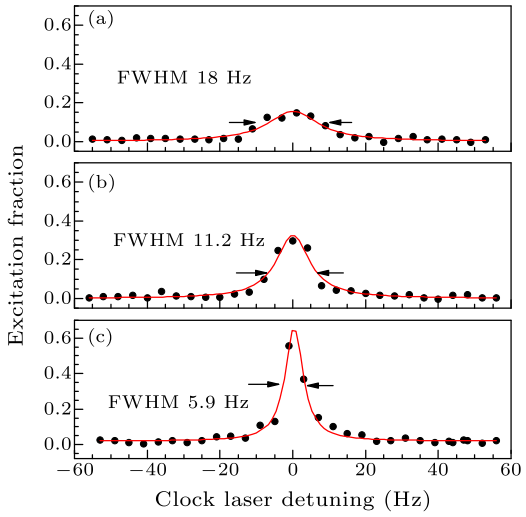

Fig. 7. The clock transition spectra with various interrogation times. (a) With 50 ms interrogation time, the linewidth is fitted to be 18 Hz. (b) With 80 ms interrogation time, the linewidth is fitted to be 11.2 Hz. (c) With 170 ms interrogation time, the linewidth is fitted to be 5.9 Hz. The experimental data are shown as the black filled circles and the Lorentz fitting results are shown as the red solid lines.

In summary, we have presented a detailed experimental study about how to realize an ultra-narrow clock spectroscopy of ^{171}Yb atoms in the 1D optical lattice. About 4×10^4 atoms are loaded into the 1D optical lattice and a lifetime of 3 s is realized at a typical lattice power of 1 W. The parameters of the optical lattice are inferred from the motional sideband spectrum, and the dependence of the carrier linewidth on the clock laser power is discussed in detail. Furthermore, the spin polarization with 95% efficiency has been realized by using a circularly-polarization laser at 556 nm. Lastly, ^{171}Yb clock spectroscopy with a Fourier-limited linewidth of 5.9 Hz is successfully obtained. These results represent a key step toward an ytterbium optical clock with high frequency stability. Further narrowing of the clock spectrum and close-loop locking of ^{171}Yb lattice clock are under way.

References

[1] Nicholson T L, Campbell S L, Hutson R B, Marti G E, Bloom B J, McNally R L, Zhang W, Barrett M D, Safronova M S, Strouse G F, Tew W L and Ye J 2015 *Nat. Commun.* **6** 6896
[2] Bloom B J, Nicholson T L, Williams J R, Campbell S L, Bishof M, Zhang X, Zhang W, Bromley S L and Ye J 2014 *Nature* **506** 71
[3] Hinkley N, Sherman J A, Phillips N B, Schioppo M, Lemke N D, Beloy K, Pizzocaro M, Oates C W and Ludlow A D 2013 *Science* **341** 1215
[4] Huntemann N, Lipphardt B, Tamm C, Gerginov V, Weyers S and Peik E 2014 *Phys. Rev. Lett.* **113** 210802
[5] Blatt S, Ludlow A D, Campbell G K, Thomsen J W, Zelevinsky T, Boyd M M, Ye J, Baillard X, Fouche M, Targat R L, Brusch A, Lemonde P, Takamoto M, Hong F L, Katori H and Flambaum V V 2008 *Phys. Rev. Lett.* **100** 140801
[6] Derevianko A and Pospelov M 2013 *Nat. Phys.* **10** 12
[7] Chou C W, Hume D B, Rosenband T and Wineland D J 2010 *Science* **329** 1630
[8] Ludlow A D, Boyd M M, Ye J, Peik E and Schmidt P O 2015 *Rev. Mod. Phys.* **87** 637
[9] Takamoto M, Hong F L, Higashi R and Katori H 2005 *Nature* **435** 321
[10] Sherman J A, Lemke N D, Hinkley N, Pizzocaro M, Fox R W, Ludlow A D and Oates C W 2012 *Phys. Rev. Lett.* **108** 153002
[11] Zhang M J, Zhang X, Liu H, Xiong Z X, Lv B L and He L X 2014 *Chin. Phys. Lett.* **31** 086701
[12] Long Y, Xiong Z X, Zhang X, Zhang M J, Lu B L and He L X 2013 *Chin. Phys. Lett.* **30** 073402
[13] Zhao P Y, Xiong Z X, Long Y, He L X and Lu B L 2009 *Chin. Phys. Lett.* **26** 083702
[14] Lemke N D, Ludlow A D, Barber Z W, Fortier T M, Diddams S A, Jiang Y, Jefferts S R, Heavner T P, Parker T E and Oates C W 2009 *Phys. Rev. Lett.* **103** 063001
[15] Droste S, Ozimek F, Udem T, Predehl K, Hansch T W, Schnatz H, Grosche G and Holzwarth R 2013 *Phys. Rev. Lett.* **111** 110801
[16] Lemke N D 2012 PhD Dissertation: *Optical Lattice Clock with Spin-1/2 Ytterbium Atoms* (Colorado: University of Colorado)
[17] Friebel S, D'Andrea C, Walz J, Weitz M and Hansch T W 1998 *Phys. Rev.* A **57** 1
[18] Blatt S, Thomsen J W, Campbell G K, Ludlow A D, Swallows M D, Martin M J, Boyd M M and Ye J 2009 *Phys. Rev.* A **80** 5
[19] Riehle F 2004 *Frequency Standards* (Weinheim: Wiley-VCH) p 147